UC Office of the President
Recent Work

Title
Room Temperature 2D Memristive Transistor withOptical Short-term Plasticity

Permalink
https://escholarship.org/uc/item/5p357771

Author
Banerjee, Kaustav

Publication Date
2018-01-25

Peer reviewed

eScholarship.org Powered by the California Digital Library
University of California

Room Temperature 2D Memristive Transistor with Optical Short-term Plasticity

Xuejun Xie[1], Jiahao Kang[1], Yongji Gong[2], Pulickel M. Ajayan[2] and Kaustav Banerjee[1,*]
[1]Department of Electrical and Computer Engineering, University of California, Santa Barbara, CA; * Email: kaustav@ece.ucsb.edu
[2]Department of Materials Science and Nanoengineering, Rice University, Houston, TX

***Abstract*—**Memristive devices with short-term plasticity (STP), gate tunability, site controllability, and light sensitivity have generated significant interest for wide range of applications, especially mimicking the neural network. However, there is still no memristive device that can accomplish all those goals in tandem at room temperature. To fill that void, in this work, 1T-phase quantum dot superlattice is created on 2H-phase monolayer single crystal molybdenum disulfide (MoS_2) back-gated field-effect transistor by focused electron beam irradiation. The quantum dots work as charge traps that induce memristive resistance. The memristive resistance can be controlled by applying gate bias and shows STP to light stimulation. Thus, this work demonstrates the first room temperature light sensitive memristive transistor that can serve as artificial retina device for artificial intelligence, and memristive receiver for optical-electrical neuromorphic interface.

I. Introduction

Memristive devices are promising artificial neuron devices for neuromorphic computing and machine learning [1], [2]. Memristive devices that have short-term plasticity (STP, where the memory spontaneously decays after stimulation) are being pursued to mimic the synaptic connection [3]. Z. Wang *et al.* used diffusive Ag-in-oxide memristive device to create STP [4]. However, this technique can only be applied to two terminal devices. Multiple terminal memristive devices or memristive transistors can bring a wider range of applications [5], [6]. However, those memristive transistors are based on random grain boundaries where the site is not controllable, and therefore not practical for large-scale integrated circuits. On the other hand, the biggest applications of neuromorphic computing are image processing and recognition, i.e., the "eyes" of artificial intelligence [7], [8]. For human eyes, the neurons are not only light sensing devices but also assemble an image processor [9], [10]. However, all the crossbar memristive devices, in principle, cannot respond to light stimulation. P. Maier *et al.* created an electro-photo-sensitive memristive device with InAs quantum dot array on two-dimensional electron gas based on GaAs/AlGaAs heterostructure [11], [12]. The quantum dots trap charges and decay with light stimulation and carrier flow, which mimics the working principle of the retina rod cell as illustrated in **Fig. 1a**. However, this device only works in cryogenic low temperature. In this work, we report a memristive transistor based on precisely designed quantum dot superlattice on single crystal monolayer MoS_2 that is controllable with gate, works at room temperature and shows a memristive STP to light stimulation. The advantages of this device are summarized in **Table 1**.

II. Material Preparation

The MoS_2 atomic layers are synthesized via chemical vapor deposition method (CVD) by using sulfur (S) and molybdenum oxide (MoO_3) powder as the precursors on Si/SiO_2 substrate. We perform the focused electron beam (FEB) irradiation on the monolayer MoS_2 with FEI XL-30 SIRION Scanning Electron Microscope (SEM) with Nanometer Pattern Generation System (NPGS) to manipulate the electron beam. The electron beam voltage is 30 kV, and the beam current is 580 pA with 2.1 nm spot size. As illustrated in **Fig. 1b**, the quantum dots are postioned in a square superlattice with 6.68 nm distance, and the size of the quantum dot is controlled by the point dose [13]. The fabricated device is shown in **Fig. 1c**. The gate dielectric is 285 nm SiO_2 with highly n-doped silicon substrate as backgate. The contact electrodes are made of 10/100 nm Ti/Au. The AFM measurement (**Fig. 2a**) indicates that the MoS_2 film is uniform and monolayer. **Fig. 2b** is the Kelvin Probe Force Microscopy (KPFM) measurement of the same region, where the FEB irradiated MoS_2 shows larger contact potential difference (V_{CPD}) compared to pristine MoS_2, which implies larger work function. As shown in **Fig. 3a** and **Fig. 3b**, the FEB irradiated MoS_2 shows larger selected area electron diffraction (SAED) peak wavenumber, and exhibits three new peaks in Raman spectrum [14]–[17]. All those evidences point to the existence of 1T-phase (metallic) MoS_2. **Fig. 3c** shows that the new PL peak emerges from the FEB irradiated MoS_2, due to the creation of 1T-phase quantum dots in 2H-phase (semiconducting) MoS_2. As shown in **Fig. 1c**, five devices are fabricated on the same MoS_2 grain with different FEB point doses of 28.6 fC, 114.3 fC, 228.7 fC, 457.4 fC, respectively, in addition to a pristine device. All the subsequent electrical measurements are conducted in 4.2×10^{-5} mBar vacuum. As shown in **Fig. 4a** and **Fig. 4b**, the FEB irradiated transistors show larger threshold voltage (V_T). The work function change and V_T shift are illustrated in **Fig. 4c**. The 2H-phase MoS_2 is originally an n-type doped semiconductor. The FEB irradiated regions transform from semiconducting 2H-phase MoS_2 to metallic 1T-phase MoS_2. The metallic quantum dots attract abundant electrons in the conduction band of adjacent 2H-phase to fill the ground state energy level of the quantum dots. As a result, the conduction band of 2H-phase MoS_2 has less electrons and the Fermi level moves towards the valance band. As the irradiation dose increases, the quantum dot size increases. For larger quantum dots, the ground state energy of electrons (holes) has smaller (larger) energy, so the material's work function increases and the V_T increases.

III. Memristive Response

Four probe measurement is carried out to extract the resistance of FEB irradiated MoS_2 excluding the contact resistance by measuring the sense voltage (V_{ds}) on V_{ds} electrodes with force voltage (V_f) and current (I) applied on V_f electrodes (**Fig. 1b**). The device is first measured with different V_f ranges without applying gate bias. As shown in **Fig. 5a** and **Fig. 5b**, the V_{ds} exhibits a hysteresis w.r.t sweeping forward and sweeping backward. As the V_f sweeping range increases from 1 V to 80 V, the hysteresis or memristive loop expands. The main mechanism controlling the hysteresis is the trapping and de-trapping of charges. There are two factors: Factor 1, as the V_f increases, the Fermi level moves down and trapped holes increase, which increases the resistance. Factor 2, as the current flows, the trapped holes decrease by recombining with mobile electrons, which reduces the resistance. When the V_f sweeps from negative to zero, the electrons are trapped near the "D" electrode as illustrated in **Fig. 5d**. When the V_f= 0 V, as illustrated in **Fig. 5e**, the trapped electrons are detected as residual V_{ds} as marked with blue dots in **Fig. 5a** and **Fig. 5b**. When the V_f sweeps from zero to a positive value, the quantum dots near the "D" electrode are charged with holes. The trapped holes reduce the Fermi level as illustrated in **Fig. 5f**. Factor 1 is saturated when all the traps are filled with holes, while the factor 2 increases as the current increases along with V_f. So the resistance reaches a saturation and starts to decrease at high V_f as shown in the inset of **Fig. 5c**. This is more significant when more electrons are generated by light as shown in **Fig 6b**. When the V_f sweeps from positive to zero, trapped holes in factor 1 decreases, and the factor 2 further reduces the holes. So the resistance decreases faster while sweeping backward and doesn't overlap with the resistance curve while sweeping forward. When V_f = 0 V while sweeping backward, as illustrated in **Fig. 5f**, the residual trapped electrons and holes is also detected as residual voltage as marked with orange dots in **Fig. 5a** and **Fig. 5b**. The number of trapped charges decaying with time can generally be formulated as $n = Ne^{-\alpha t}$, where N is the total number of the trapped charges and α is the decay coefficient. The trapped charges generally decay faster at higher temperatures, which implies larger α. In the case of quantum dot based memristive device in previous works [11], [12], only few quantum dots are created. Hence, those devices require cryogenic low temperature to maintain memristive behavior. In our case, the quantum dots are closely positioned in a square superlattice with 6.68 nm distance, which implies large N. Moreover, the monolayer 2D materials (in our case MoS_2) are extremely sensitive to the trapped charges [18], [19]. That's the reason why our quantum dot based memristive device exhibits memristive behavior even at room temperature. As demonstrated in **Fig. 5a**, this memristive device can work at very low voltages, which can dramatically reduce the power consumption. In this case, the V_{ds} can be as low as 10^{-4} V for a 2.1 μm channel. Reducing the channel length can further reduce the voltage requirements. In order to better visualize the memristive behavior, we still choose 80 V as the V_f sweeping range in the subsequent measurements.

IV. Light response

Another interesting property of this memristive device is the gate tunability and light responsiveness. The measurement is conducted with light (halogen light) ON and OFF under different back gate voltages (V_G). The resistance R is extracted by calculating V_{ds}/I as shown in **Fig. 6a** and **Fig. 6b**. The MoS_2 is natively n-type doped with a threshold voltage of 20 V. When V_G > 20 V, all the quantum dots are charged with electrons as illustrated in **Fig. 6c**, so the R doesn't have a memristive loop. When the light is ON, the light-induced electrons and holes fill up all the quantum dots. Thus, the memristive response is also suppressed as illustrated in **Fig. 6d**. When the V_G is largely negatively biased, the memristive response starts to emerge even with the light ON.

The interesting response to light stimulation is further examined with modulating light illumination during the V_f sweeping as shown in **Fig. 7**. The V_f sweeps from -80 V to 80 V to -80 V with no gate bias. The light is mechanically blocked to switch OFF. In **Fig. 7a** and **Fig. 7b**, during the V_f sweeping, the R exhibits gradually rising peaks when the light is OFF. When the light is ON, the R exponentially decreases and progresses to a stationary value that is in between the light-always-on and light-always-off data. In other words, the device shows memristive response to V_f sweeping and STP to the light stimulation. This can be explained as shown in **Fig. 7c**. The main factor which increases the R is the trapped holes that move the local Fermi level towards lower energy. The main factors that decrease R are the light generated electrons and the recombination of trapped holes with electrons. When the V_f is supplying positive voltage, the holes are constantly generated near the "S" electrode. When the light is ON, the electrons and holes are generated by light, which leads to low R. When switching to light-OFF, electrons and holes recombine and some holes are trapped, and the increasing of V_f further increases the trapped holes, which gradually increases the resistance. When switching to light ON, the electron and holes are generated, and the trapped holes recombine with mobile electrons. This process reduces the resistance, which is the origin of STP. When V_f = 80 V, the device reaches a resistance that is larger than the light-always-on condition and smaller than the light-always-off condition. In other words, the device "remembers" the history of the light stimulation.

V. Summary

A room temperature light memristive transistor is created on monolayer single crystal MoS_2. This is achieved by creating a 1T-phase MoS_2 quantum dot superlattice on 2H-phase MoS_2 using FEB irradiation. As the FEB irradiation dose increases, the material's work function increases, and the transistor's threshold voltage moves to larger values. Four probe measurements confirm that the transistor exhibits a memristive resistance corresponding to drain voltage sweeping and STP to light stimulation. Thus, this work demonstrates the first room temperature light sensitive memristive 2D-channel transistor that can serve as artificial retinal device for artificial intelligence, and memristive receiver for optical-electrical neuromorphic interface.

Acknowledgment

This work was supported by the AFOSR (grant FA9550-14-1-0268), the NSF (grant ECCS-1550230) and the UC Lab Fee Research Program (grant LFR-17-477237).

References

[1] L. Chua, "Memristor-The missing circuit element," *IEEE Trans. Circuit Theory*, vol. 18, pp. 507–519, 1971.

[2] D. B. Strukov, G. S. Snider, D. R. Stewart, and R. S. Williams, "The missing memristor found," *Nature*, vol. 453, pp. 80–83, 2008.

[3] T. Ohno, T. Hasegawa, T. Tsuruoka, K. Terabe, J. K. Gimzewski, and M. Aono, "Short-term plasticity and long-term potentiation mimicked in single inorganic synapses," *Nat. Mater.*, vol. 10, pp. 591–5, 2011.

[4] Z. Wang *et al.*, "Memristors with diffusive dynamics as synaptic emulators for neuromorphic computing," *Nat. Mater.*, vol. 1, Sep. 2016.

[5] P. Maksymovych *et al.*, "Dynamic conductivity of ferroelectric domain walls in $BiFeO_3$," *Nano Lett.*, vol. 11, pp. 1906–12, 2011.

[6] V. K. Sangwan *et al.*, "Gate-tunable memristive phenomena mediated by grain boundaries in single-layer MoS_2," *Nat. Nanotechnol.*, vol. 10, pp. 403–406, 2015.

[7] M. Prezioso, F. Merrikh-Bayat, B. D. Hoskins, G. C. Adam, K. K. Likharev, and D. B. Strukov, "Training and operation of an integrated neuromorphic network based on metal-oxide memristors," *Nature*, vol. 521, pp. 61–64, 2015.

[8] Y. LeCun, Y. Bengio, and G. Hinton, "Deep learning," *Nature*, vol. 521, no. 7553, pp. 436–444, May 2015.

[9] J. Lettvin, H. Maturana, W. McCulloch, and W. Pitts, "What the Frog's Eye Tells the Frog's Brain," *Proc. IRE*, vol. 47, pp. 1940–1951, Nov. 1959.

[10] J. E. Dowling and F. S. Werblin, "Synaptic organization of the vertebrate retina," *Vision Res.*, vol. 11, Jan. 1971.

[11] P. Maier *et al.*, "Electro-Photo-Sensitive Memristor for Neuromorphic and Arithmetic Computing," *Phys. Rev. Appl.*, vol. 5, p. 54011, May 2016.

[12] P. Maier *et al.*, "Light sensitive memristor with bi-directional and wavelength-dependent conductance control," *Appl. Phys. Lett.*, vol. 109, 2016.

[13] X. Xie *et al.*, "Designing artificial 2D crystals with site and size controlled quantum dots," *Sci. Rep.*, 2017. DOI: 10.1038/s41598-017-08776-3

[14] M. A. Lukowski, A. S. Daniel, F. Meng, A. Forticaux, L. Li, and S. Jin, "Enhanced hydrogen evolution catalysis from chemically exfoliated metallic MoS_2 nanosheets," *J. Am. Chem. Soc.*, vol. 135, pp. 10274–10277, 2013.

[15] S. Jimenez Sandoval, D. Yang, R. F. Frindt, and J. C. Irwin, "Raman study and lattice dynamics of single molecular layers of MoS_2," *Phys. Rev. B*, vol. 44, pp. 3955–3962, 1991.

[16] R. Kappera, D. Voiry, S. Yalcin, and B. Branch, "Phase-engineered low-resistance contacts for ultrathin MoS_2 transistors," *Nat. Mater.*, vol. 13, Aug. pp. 1128–1134, 2014.

[17] Y. Kang *et al.*, "Plasmonic hot electron induced structural phase transition in a MoS_2 monolayer," *Adv. Mater.*, vol. 26, pp. 6467–6471, 2014.

[18] D. Sarkar, W. Liu, X. Xie, A. C. Anselmo, S. Mitragotri, and K. Banerjee, "MoS_2 Field-Effect Transistor for Next-Generation Label-Free Biosensors," *ACS Nano*, vol. 8, pp. 3992–4003, Mar. 2014.

[19] D. Sarkar *et al.*, "A subthermionic tunnel field-effect transistor with an atomically thin channel," *Nature*, vol. 526, pp. 91–95, 2015.

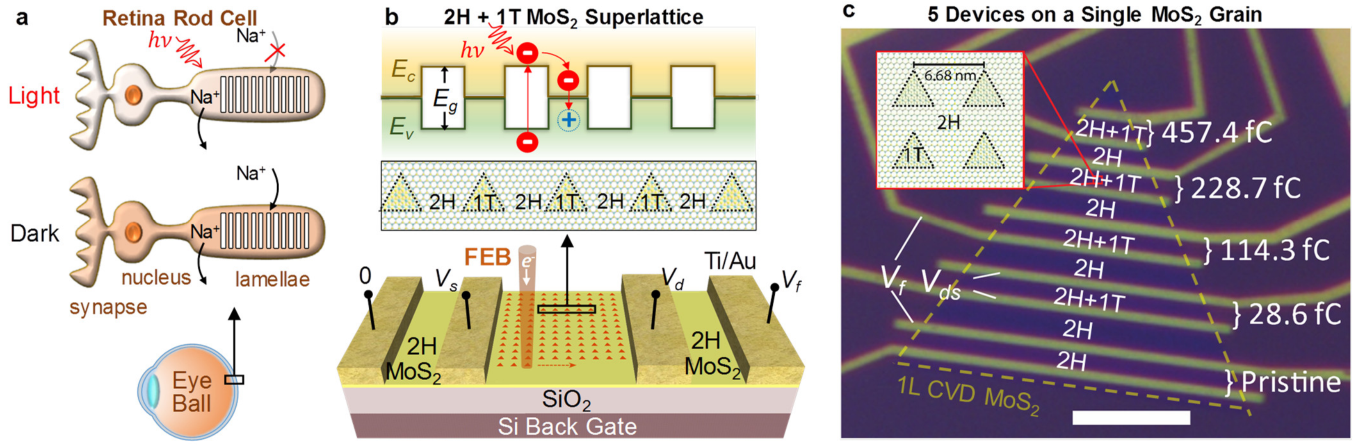

Fig. 1. **(a)** The sketch shows the working principle of retina rode cell that accumulates charges with light stimulation and reduces the charges in dark. **(b)** The schematic on the bottom shows the device structure with MoS_2 as channel, Ti/Au as contacts, SiO_2 as back dielectric and Si as backgate. The focused electron beam (FEB) creates local 1T-phase regions in 2H-phase MoS_2, which work as quantum wells in MoS_2 channel. As shown by the middle inset, the 1T regions grow in triangle shape due to the hexagonal lattice of MoS_2. The top inset shows the band diagram of the superlattice, where the 2H (E_g = 1.8 eV) and 1T (E_g = 0 eV)-phases are alternated. With light stimulation, the quantum well can trap electrons. In the dark, the trapped electron decays in the quantum wells formed by 1T dots. **(c)** The optical image of five back-gated field effect transistors (FETs) fabricated on monolayer (1L) single crystal MoS_2 grown by chemical vapor deposition (CVD). The FET channels are the FEB irradiated regions marked with bracket and corresponding irradiation point dose (in unit of fC) on the right side. The inset is the schematic of the 1T-phase MoS_2 quantum dots created by FEB irradiation in 2H-phase MoS_2. V_f and V_{ds} mark the electrodes for force voltage and sense voltage for four-probe measurement, respectively. The white scale bar is 10 um.

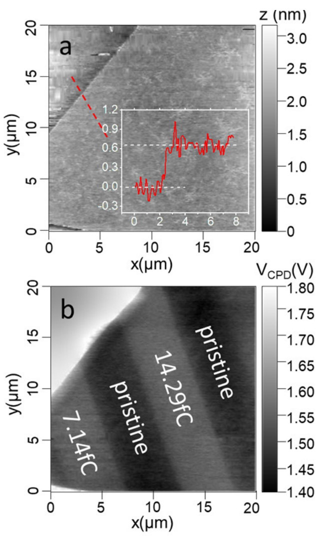

Fig. 2. **(a)** Atomic force microscope (AFM) image of the MoS_2 sample. The inset is the cross-section plot of the AFM data along the red dashed line. The average thickness of ~0.65 nm indicates monolayer. **(b)** Kelvin probe force microscopy (KPFM) image of the same region as in (a). Higher contact potential difference (V_{CPD}) implies larger work function. As the FEB irradiation dose increases, the work function of MoS_2 increases.

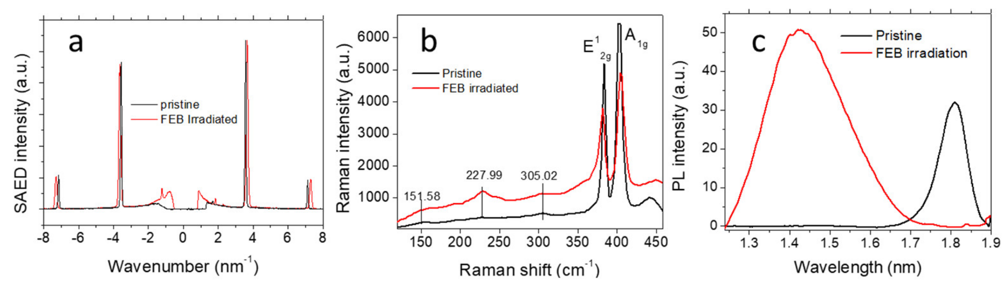

Fig. 3. **(a)** SAED measurement showing that FEB irradiated MoS_2's peaks have larger wavenumber, which is an indication of 1T phase MoS_2. **(b)** Raman spectrum showing the FEB irradiated MoS_2 has new peaks at 151.58 cm^{-1}, 227.99 cm^{-1}, and 305.2 cm^{-1}, which is a signature of 1T phase MoS_2. **(c)** PL measurement reveal the new PL peak emerge from FEB irradiated MoS_2, which can be attributed to the creation of 1T-phase quantum dots in 2H-phase MoS_2.

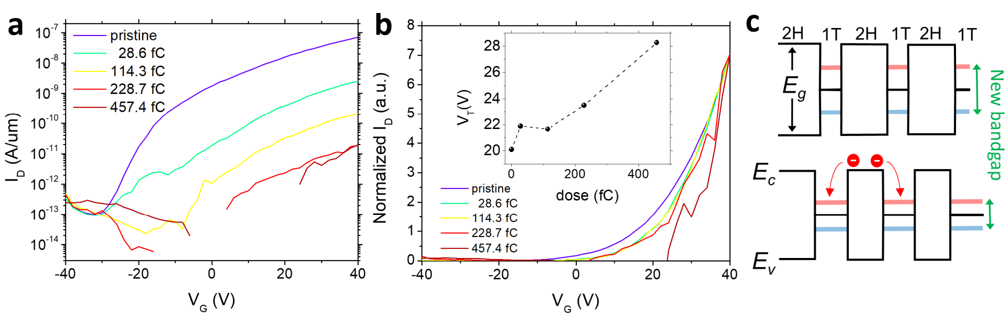

Fig. 4. **(a)** Drain current (I_D) *vs.* back gate voltage (V_G) curve for MoS_2 FETs with different irradiation doses. **(b)** The normalized I_D - V_G curve for comparing the threshold voltage (V_T). The inset shows the extracted V_T. As the irradiation dose increases, the V_T increases. **(c)** The top and bottom sketches represent the band diagrams with small and large quantum dots, respectively. As the irradiation dose increases, the quantum dot size increases. For superlattice with larger quantum dots, the ground state energy of electrons (holes) has smaller (larger) energy, so the work function increases and the V_T increases.

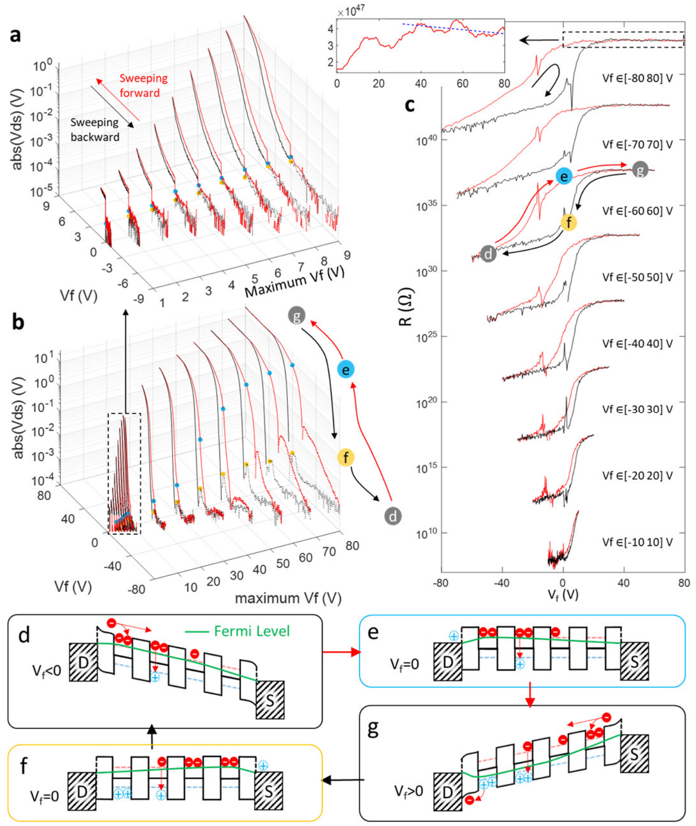

Fig. 5. FEB irradiated transistor characterization. **(a), (b)** abs(V_{ds}) *vs.* V_f with different V_f sweeping range. The red line is the data for V_f sweeping forward from – to +. The black line is the data for V_f sweeping backward from + to –. The dashed lines are data with negative value. The blue and orange dots mark the data when the V_f = 0 V for V_f sweeping forward and backward, respectively. **(c)** The resistance (R) *vs.* V_f. To better visualize the result, the data is calculated with $R \times 10^{[\max(V_f)-10]/2}$ to separate the data in vertical direction for different V_f sweeping range. **(d), (e), (f), (g)** illustrate the working principle. As the V_f increases, the Fermi level moves down and trapped holes increase, which increases the resistance. As the current flows, the trapped holes decrease by recombining with mobile electrons, which reduce the resistance.

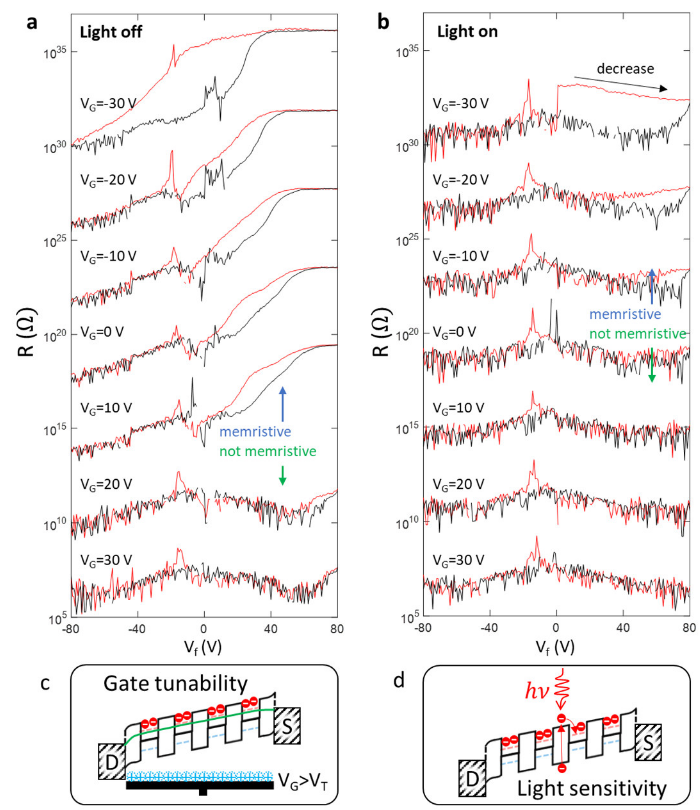

Fig. 6. Measurements demonstrating the gate tunability and light sensitivity. **(a)** I *vs.* V_f with different back gate voltage (V_G) with light ON. **(b)** I *vs.* V_f with different V_G with light OFF. To better visualize the result, the data in (a) and (b) are calculated with $R \times 10^{(30-V_G)/2.5}$ to separate the plot in vertical direction for different V_G. The memristive response can be reduced with applying positive gate voltage or light stimulation. **(c)** When the V_G > V_T, the quantum dots are filled with electrons, which eliminate the memristive loop. **(d)** When the light is constantly on, the quantum dots are also filled with electrons, which eliminate the memristive loop, unless a larger gate voltage reduces the electrons.

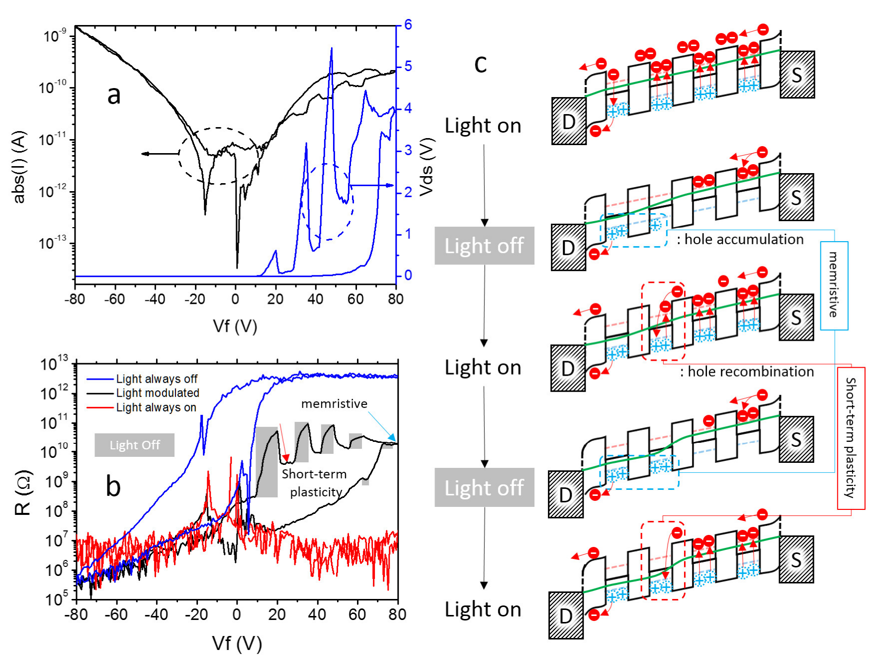

Fig. 7. Light response. **(a)** The absolute value of I in log scale and V_{ds} as the function of V_f for light modulated condition with no gate bias. The light OFF regions are marked in (b). **(b)** The R as the function of V_f for light always ON, light always OFF, and light modulated condition, where the resistance for light modulated condition is calculated from (a). The gray regions are when the light is OFF for light modulated condition. **(c)** The memristive loop is due to hole generation during the light OFF. The optical short-term plasticity is due to the hole recombination during the light ON.

Table 1. The advantages of this work compared to previous studies.

	Refs. (3)(4)	Refs. (5)(6)	Refs. (7)(8)	**This Work**
STP	✓			✓
Gate tunability		✓		✓
Site controllability	✓		✓	✓
Light sensitivity			✓	✓
Room temperature operation	✓	✓		✓